

Developments on the Hybrid Stiffness - Flow Control Active System for Rotor Vibration Attenuation Project – SHARCS

Fred Nitzsche*, fred_nitzsche@carleton.ca

Daniel Feszty

Fatma Demet Ulker

Melissa Richardson

Carleton University, Canada

*Guest Scientist at the German Aerospace Center (DLR)
Institute of Composite Structures and Adaptive Systems, Germany

Steve Vamosi

Alex Pickard

Kostyantyn Khomutov

Smart Rotor Systems Inc., Canada

Abstract

At Carleton University's rotorcraft research group, we are working since 2003 in the development of an active rotor control system that incorporates a mechanism for blade pitch compliance adaptation at the root, the active pitch link and an on-blade flow-control actuation mechanism, the actively controlled flap. The objective is to employ a hybrid rotor control concept (SHARCS, acronym for "Smart Hybrid Active Rotor Control System") comprised by these two subsystems to attenuate the aeroelastic response of the blade at the frequencies of interest. We believe that the cooperation between these two subsystems will vastly expand the capability of smart material systems to overcome their intrinsic stroke limitations and to attain superior performance in performing individual blade control for rotor vibration alleviation. The two subsystems are being presently developed at the whirl tower built by Carleton University on the grounds of the National Research Council Canada (NRC). This paper will report the most recent achievements in producing both the hardware and software of the SHARCS system tailored to a dynamically similar 1-meter span hinged rotor blade model.

1. INTRODUCTION

Most of the current active vibration control research activities attempt to actively alter the time varying aerodynamic loads on the blade to suppress vibration. However, successful implementation of this approach has been hindered by electromechanical limitations of piezoelectric material actuators such as their small stroke. An impedance control device was designed to adaptively alter the stiffness, damping and effective mass of the blade to control the structural response. One example of such mechanism is shown in the conceptual drawing in Fig 1, optimized to exploit the large force delivered and the frequency bandwidth of piezoelectric materials to perform an indirect-active vibration control of the axial loads generated at the "structure" that are transmitted to the "base." The primary advantage of this system (nicknamed "smart spring") when compared to other piezoelectric actuator based approaches is that the device does

not rely on the piezoelectric actuators to achieve high stroke and force simultaneously (meaning high power and high required voltages). Rather, the device only requires the actuators to produce micro displacements to generate relatively high actuation forces. As such, the stacked piezoelectric actuators are able to achieve sufficient forces with less than 100V (volts) peak-to-peak.

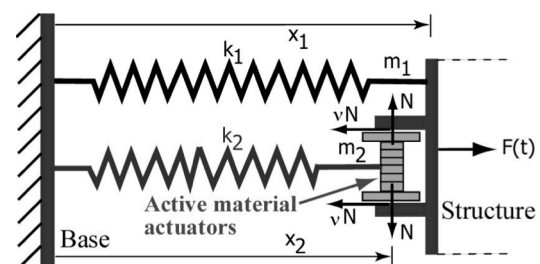


Fig. 1: Axial impedance control device.

The “smart spring” device was already extensively reported in other publications as a mean of reducing helicopter blade vibration.^{[1]-[7]} In Section 2, a brief overview of its operation is given for the sake of completeness. In the SHARCS project, the “smart spring” is inserted between the blade horn and the rotor swashplate, hence replacing the conventional pitch link to perform IBC and reduce the transmitted vibration between the rotating to the non-rotating frames.^[8] For this reason, it is referred in this paper as the *active or adaptive pitch link*, APL (Fig. 2). It is very important to stress that the APL does not produce significant angles of attack. In fact, they were measured to be less than 0.1 degrees in the experiments reported in this paper. Therefore, the IBC system pursued in SHARCS is unconventional in the sense that no angle of attack is introduced at the root of the blade to generate aerodynamic loads. Vibration reduction is achieved in SHARCS by actively altering the torsional boundary condition of the blade, thereof providing a *parametric excitation of the elastic degrees of freedom of the blade*. For this reason, the APL is referred in SHARCS as a *stiffness control* device. This latter idea will also be discussed in more details in Section 2, along with the results obtained in bench (non-rotating) tests with a closed-loop control law. In Section 3, the tests obtained in the whirl tower with the APL using an open-loop control law are reported.

The ACF (actively controlled flap) is introduced in SHARCS as a *flow control* device to reduce either vibration or noise, depending on the actuation schedule. As opposed to the APL, the ACF control authority is linked to its ability to produce significant deflections (hence aerodynamic loads) at the desired control frequencies. The ACF is rectangular with dimensions spanning from 65% to 85% along the blade radius and 15% along the chord, from the trailing edge. This geometry was identified by as the most efficient combination in terms of (a) aerodynamic efficiency, for which the flap should be as much outboard as possible but not beyond the 90% radius where tip losses dominate and, (b) the aerodynamic power efficiency, for which the 15% chord length flap was shown to be the optimum.^[9] The maximum desired actuation frequency is of at least 5/rev for the SHARCS 4-bladed rotor. Although the desired flap deflection amplitude is deemed to be as large as possible, achievable values in the best designs for reduced-scale blades were reported in the range of 4-6 degrees in the non-rotating condition. In Section 4 a closed-loop control system for vibration reduction using this deflection limitations was investigated using a high-fidelity aeroelastic simulation tool.

As stated, SHARCS incorporates both a *stiffness control* device (APL) and a *flow control* device (ACT), thereof it is here classified as a *hybrid* IBC

system, where the *stiffness control* system is designed to reduce vibrations and the *flow control* device is designed to either further reduce vibrations that could not be damped by the APL (such as those independent from the elastic torsion of the blade) or, alternatively, to attenuate rotor noise without the compromise of increasing vibrations, as often was reported in the literature.^[10] In Section 5, the conclusions of the present paper are presented.

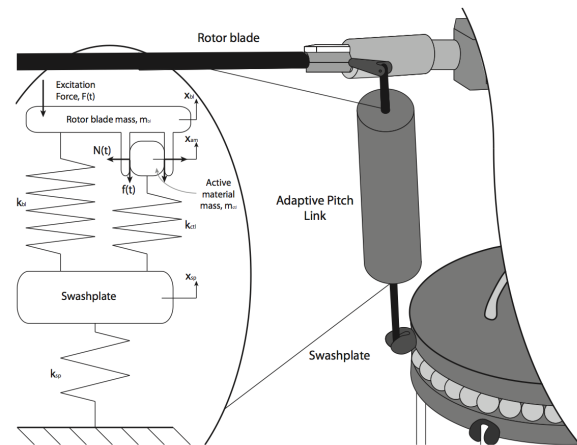


Fig. 2: Active Pitch Link.

2. BLADE STIFFNESS CONTROL BY AN ACTIVE PITCH LINK

It is important to understand that the active pitch link (APL) is based on the “smart spring” concept and relies on delivering power not to actuate against the aerodynamic loads but to change the *effective spring constant* of the device (or, more precisely, its impedance). It is the change of the flexural torsional characteristics of the blade (throughout its boundary conditions) that allows the control of the aeroelastic response of the system. Energy is redistributed in the spectrum of vibration, removed from the frequencies where the transmissibility is desired to be low (i.e. at the frequencies integer multiples of the number of blades, n/rev and their immediate neighbors) and displaced it at frequencies known to have lower transmissibility in the helicopter rotor. Therefore, such a device is able to control the blade aeroelastic response in an *indirect* way. The primary advantage in the APL system, compared to conventional IBC systems, is that the APL does not rely on the actuators to achieve high stroke and force simultaneously. Rather, the device only requires the piezoelectric actuators shown in Fig. 1 to produce micro displacements to close the initial gap between the stacked actuators and the sleeve connected to the “structure.” The gap is kept as low as possible to maximize the actuation force, N that produces the friction force vN between the two surfaces. This friction force ideally should be enough

to guarantee that there is no sliding between the actuators and the sleeve and, therefore, $x_1 = x_2$ at the times when the springs are perfectly engaged, $k = k_1 + k_2$. However, even when some sliding exists the device is able to perform stiffness modulation because a dynamic (complex-valued) equivalent spring constant is created due to the Coulomb friction between the two surfaces, $k = \text{Re}(k) + i\text{Im}(k)$. This “damping effect” is beneficial to the system stability because part of the mechanical energy is converted into heat. In the experiments, instability of the system was never observed. Nevertheless, it must be noted that for security reasons (fail safeness) in the practical implementation of the device the situation $k = k_1 + k_2$ occurs when the applied voltage is zero. Hence, the actuators are used to *disengage* the two springs *rather than engaging* them (assume in Fig. 1 that the actuators contract rather than expand for non-zero voltages, opening the gap and leaving only the primary spring, k_1 in the load path). Furthermore, in order to modulate the dynamic response of the blade, the device is evidently more effective if placed near the root to actively alter its boundary conditions, which may instantaneously change from a perfect inelastic connection to the swashplate (if $k_2 \rightarrow \infty$) to some finite elastic value, $k = k_1$.

2.1. The stiffness modulation principle

Following the previous discussion, in the present APL design, the instantaneous stiffness is *reduced* from its maximum level, $k_1 + k_2$ to $k(\alpha)$, which is composed by the time-averaged spring constant, k_0 modulated with the amplitude of the secondary spring, k_2 (see Fig. 3). Hence:

$$(1) \quad k(\alpha) = k_0 + k_2 f(\alpha),$$

where the periodic actuation signal function, $f(\alpha)$ depends on the control frequency, ω and the control phase angle, ϕ and has zero time average. The control frequency is set at certain harmonics of the rotor fundamental frequency (the spinning rate), $\omega = p\Omega$, where p is an integer.

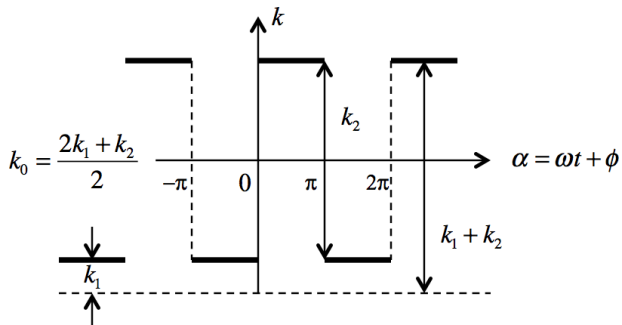


Fig. 3: APL stiffness modulation (theoretical).

The harmonics of $f(\alpha)$ are responsible for reshaping of the vibration spectrum, spreading the vibration energy at multiples of the fundamental frequency. In the case of the square wave control signal shown in Fig. 3:

$$(2) \quad f(\alpha) = \frac{2}{\pi} \left(\sin \alpha + \frac{\sin 3\alpha}{3} + \frac{\sin 5\alpha}{5} + \dots \right).$$

This principle becomes clearer if one recalls the first-order dynamic system parametric excitation, which is generally described by Hill's equation:

$$(3) \quad m\ddot{x} + k(t)x = F(t).$$

This equation can be seen as the dynamic equivalent of the “smart” spring (Fig. 1), valid at any instant of time, where $m = m_1$ is the mass of the “structure” and the hanging mass is negligible, $m_2 \equiv 0$. A special case of (3) is the well-known Mathieu's equation, where the stiffness modulation is purely sinusoidal. This equation provides a form of *parametric* excitation of the system. In the present case, the external force $F(t) = F_n \sin(n\Omega t)$ is the n^{th} harmonic of the fundamental frequency, Ω whose control objective is to reduce the forced response (uncontrolled) amplitude, $x(t) = x_n \sin(n\Omega t)$. Using (1) and (3) and neglecting for the sake of simplicity the contributions from both the lower- and higher-order harmonics of the fundamental frequency, $(n \pm q)\Omega$, where $q = 1, 2, \dots$:

$$(4) \quad x_n = \frac{F_n/k_0}{1 + m/k_0(-n^2\Omega^2 + k_2/m f(\alpha))}.$$

The latter expression interestingly shows the natural harmonic control character of the “smart” spring (and so the APL) because the following closed-loop feedback block diagram formally represents (4):

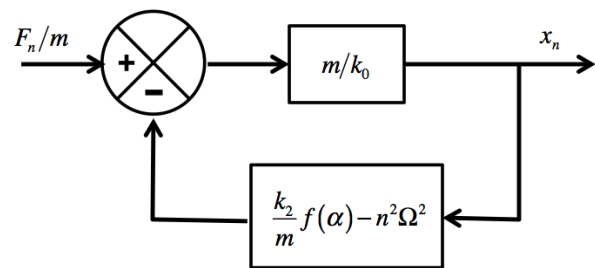


Fig. 4: APL block diagram.

The above block diagram can be seen as the feedback from the uncontrolled response signal from the n^{th} harmonic, F_n/k_0 to its controlled harmonic response signal, x_n throughout the APL system. Note that the latter is an output signal with *amplitude modulated in time by the control frequency*, $x_n = x_n(\alpha)$, where $\alpha = \omega t + \phi$ is the control input. Hence, the APL closed-loop control objective is achieved by

adjusting the control input, α (i.e. the control frequency, ω and the control phase, ϕ) in (4). The final vibration response amplitude, x_n can be either increased or decreased in magnitude according to the control input due to the structure of (4), where the feedback signals may alternate according to the control input α and the relative magnitudes of $n^2\Omega^2$ and k_2/m . Note that the contributions from the higher harmonics of the control input signal (frequency and phase) to the control objective actually decrease monotonically as odd multiples of the control frequency, ω following the denominators in the series expansion shown in (2).

Therefore, the objective of a suitable closed-loop control law in the present IBC system scheme is to decrease the dynamic response at the critical harmonics of the fundamental frequency (associated with the integer multiples of the number of blades and their immediate neighbors) neither affecting the rotor mean thrust (the collective control at 0/rev) nor the blade azimuth pitch control system (cyclic control at 1/rev).

In the present paper, two controlled cases will be presented: in Section 2.4, the APL was excited in the bench by an electromagnetic shaker and a simple closed-loop control law was realized to decrease the transmitted loads; in Section 3, the APL replaced the conventional blade pitch link in whirl tower tests. The control harmonic number and the relative phase, respectively $p = \omega/\Omega$ and ϕ in α were varied in only two open-loop control cases, for $p = 1, 2$. Hence, *no optimization was attempted to follow the stated principles of a suitable control law for helicopter rotors*. The tests were performed only to prove the principle of stiffness modulation and to show the reshape of the blade response spectrum measured in the non-rotating frame.

2.2. Active pitch link (APL) hardware

Over the past ten years, three prototype active pitch links (APL) were developed. The first prototype, developed in 2003, was a large-scale system to prove the concept, Fig. 5(a). Hence, no effort was made to meet any design requirement such as size and fail safeness. The second generation of APL was manufactured in 2006, Fig. 5(b). This design was already very compact (0.108m long) with adjustable preload settings and a total mass of 0.196 kg to fit the 1-m SHARCS blade. After testing this unit in both non-rotating and whirl tower tests the present third generation of the APL prototype was designed and built in 2010, Fig. 5(c). It incorporates a clamp mechanism whose operation is largely independent from the centrifugal loads for improved performance in the rotating tests. In the last prototype design, the system stiffness can be varied between k_1 ("soft" link) and k_1+k_2 ("solid" link),

where $k_2 \gg k_1$ in Fig. 1. Hence, in case of power failure or malfunctioning the prototype recovers the "solid" link stiffness condition, k_2 .

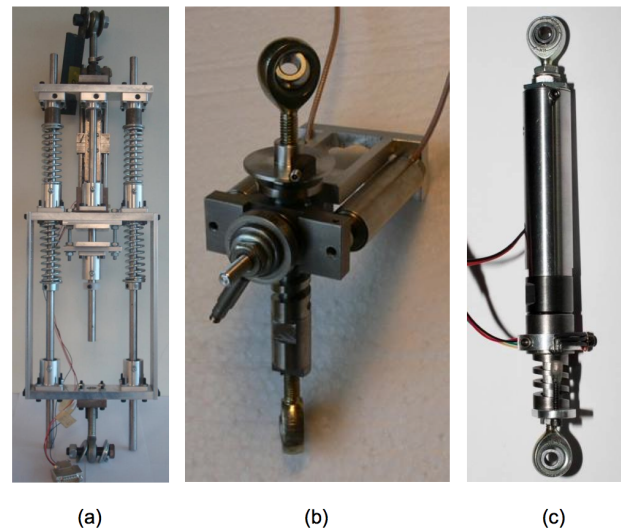


Fig. 5: APL prototypes: (a) – 1st generation, 2003, (b) – 2nd generation, 2006 and (c) – 3rd generation, 2010.

2.3. APL operation and characterization

There are three modes of operation for the APL and the input voltage sent to the piezoelectric actuator controls them. The first is the "solid" link mode, which is theoretically achieved with an input voltage in the range of 0-60V. In this mode, the stiffness of the APL is virtually infinity and it acts as the traditional solid pitch link. The second mode of operation is in "transition" range, where the APL stiffness varies from its maximum to its minimum value. An input voltage in the range of 60-120V controls this mode. The last mode of operation is the "soft" link mode, controlled by an input voltage of 120-150V. In this mode, the load path is carried through the APL softer spring resulting in the design stiffness of 160kN/m.

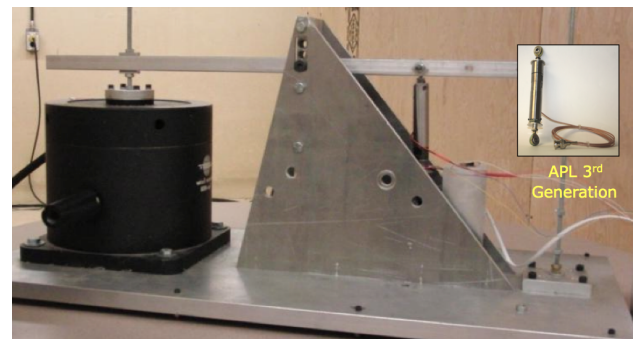


Fig. 6: APL non-rotating bench tests.

The APL stiffness curve is a plot of the calculated resultant stiffness as a function of the piezoelectric

input voltage. To create this plot, an external dynamic load was applied axially to the APL by an electromagnetic shaker, Fig. 6. The magnitude $F = 37\text{N}$ was kept constant in the tests with a frequency of 15.7Hz . This procedure was repeated for several different piezoelectric input voltages and data was collected for ten input voltages, ranging between 15 and 150V. For each data point the time history of the displacement (measured by a Hall sensor) was recorded. This data was used to determine the magnitude of the “smart” spring displacement for each corresponding input voltage. The equivalent stiffness was then calculated using the ratio of force amplitude to the spring displacement amplitude for each input voltage (Fig. 8).

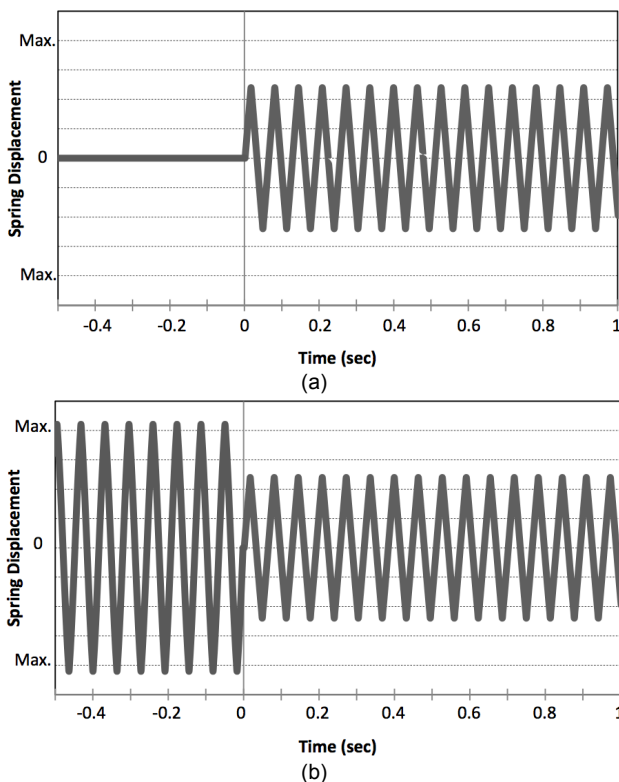


Fig. 7: APL characterization: (a) – 1st initial condition and (b) – 2nd initial condition.

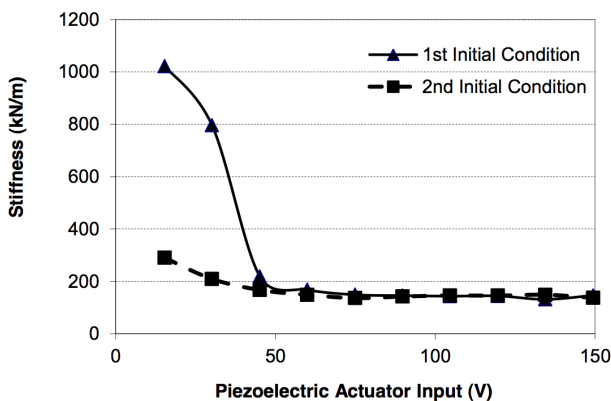


Fig. 8: APL effective dynamic stiffness.

As the APL was designed to use a friction clamp to vary the stiffness of the system, the force required to overcome a frictional force is much less for already moving parts than for initially stationary parts. For this reason, the initial conditions of the friction clamp were verified to be very important when determining the experimental stiffness curve of the APL. In order to show the effect of the initial conditions of the friction clamp, the experimental stiffness curve was developed twice: initially stationary – the “1st initial condition,” Fig. 7(a) and initially moving – the “2nd initial condition,” Fig. 7(b). The voltage was applied at $t = 0$ and the result of this procedure is summarized in Fig. 8 as the real part of the effective stiffness k versus actuator voltage curves for the two stated initial conditions. The curves shall approach asymptotically the static values of k_1 and k_2 at their lower and higher voltage branches, respectively. However, no spring displacement data was collected when the piezoelectric actuator voltage applied was zero or near zero since in this condition the APL functions as the “solid” pitch link with stiffness, k_2 and the data points became scattered and not repeatable. Nevertheless, the curves capture relatively well the transition zone of the APL, where only partial clamping occurs and there is sliding between the actuators and the sleeve (see Fig. 1). Obviously, for this particular region, the imaginary part of k is also relevant for the system identification, as it accounts for the Coulomb friction effect. However, this effect is not reported in this study.

2.4. Closed-loop control

Previous computational research demonstrated that the APL could reduce vibrations transmitted through the pitch link when a state-switch control algorithm is implemented.^[6] The scheme creates a parametric excitation of the structure by modulation of its stiffness. In the APL shown in Fig. 1, the overall stiffness is increased when the “structure” and the “base” move one against the other, absorbing the kinetic energy of the system. When the “structure” and the “base” move one away from the other no action is done. In this way, the relative motion is demoted. A “maximum extracting energy” control approach may be implemented following this approach.^[7] In the present research, however, a modified version of this control algorithm was implemented, in which the state switching event is predicted from the previous time-history of the vibration rather than using the instantaneous information through a feedback signal. Therefore, the previous knowledge of the excitation force F is necessary, which considerably restricts its use in random vibration cases but may be applicable to rotorcraft due to the periodicity of the aerodynamic loads, which at each flight condition can be indeed

“on-line” identified using, for example, neural network techniques.

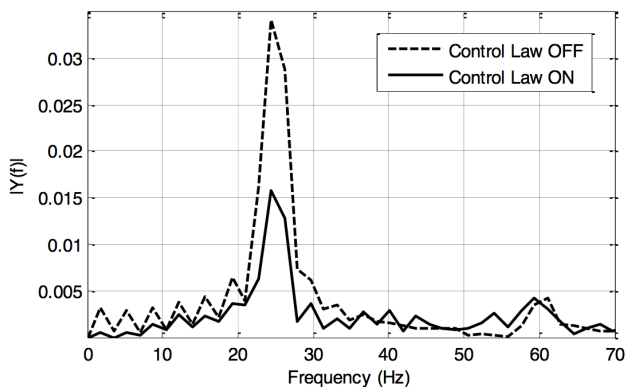


Fig. 9: APL controlled versus uncontrolled vibration spectrum. Input load: $F = 37\text{N} @ 25\text{Hz}$.

Experimental implementation of the latter proposed closed-loop control algorithm proved that in non-rotating tests the APL achieved about 60% reduction in the vibrations (peak-to-peak) transferred from the shaker through the pitch link to the “base.” It was clearly confirmed in the experiments that this reduction was due to the implementation of the stiffness modulation principle, as the APL device is stiffness controlled with an internal resonance much higher than the forced frequency of the system. Hence, the response frequency remained virtually constant in the vibrational spectrum, Fig. 9.

3. APL TESTS IN THE WHIRL TOWER

The APL was subsequently tested at the Carleton University whirl tower recently constructed on the grounds of the National Research Council Canada (NRC), Fig. 10. In the whirl tower, a single blade hinged rotor hub was installed. In the tests, the APL was positioned at its normal location, replacing the conventional pitch link, Fig. 11. The APL control voltage was fed into the rotating frame by slipping rings and the data was acquired using the wireless telemetry located inside the hub. A calibrated Hall sensor at the base of the pitch link was used to collect the vibrational data that would be transmitted into the non-rotating frame (the swashplate in the helicopter case) from the blade.

The tests were carried out at three spinning ratios (rotor fundamental frequency) of 600, 750 and 1,000RPM. Although the nominal spinning ratio of the SHARCS Mach-scaled blades is 1,550RPM, the tests were limited to this rotating speed due to current restrictions in the APL design. It was expected that the piezoelectric actuator used would not deliver enough stroke to clamp for rotating speeds of 1,000RPM and beyond due to its small size.

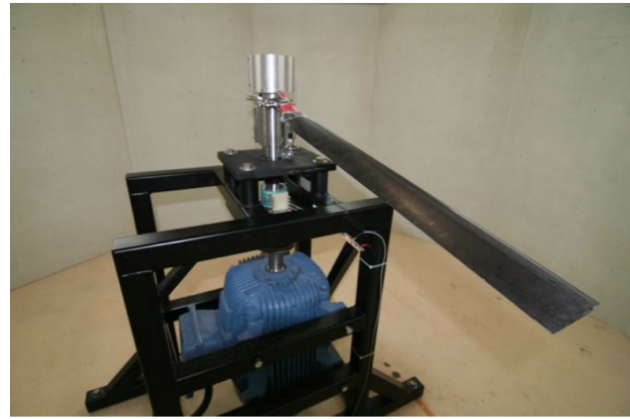


Fig. 10: Carleton University whirl-tower facility (hub, top figure and control room, bottom figure).



Fig. 11: APL installation in the rotor hub.

For these tests, a fan was positioned at the bottom of the whirl tower to provide a transverse flow with the intention to excite the blade with a periodic aerodynamic load, as in forward flight. The excitation provided by the fan was considered sufficient for at least the first 3 harmonics of the rotor fundamental frequency for all spinning ratios, as seen in Fig. 12. The centerline position of the fan, whose relative dimension is also shown in the same figure, was taken as the reference azimuth for the control signal input (0 degree control phase).

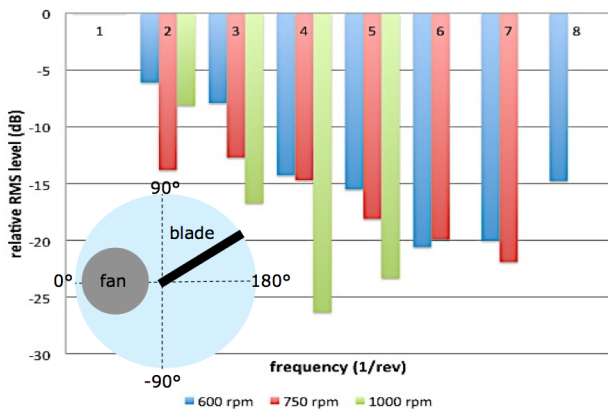


Fig. 12: Blade excitation attenuations with respect to the rotor fundamental frequency (1/rev) for different spinning ratios (RPM).

Since the purpose of the tests was to demonstrate the effectiveness of the APL to redistribute the vibration spectrum in the rotating condition, no optimization of the control law was pursued in this work. The APL design objective of not interfering with the fundamental frequency of the rotor, $\Omega = 1/\text{rev}$ was, therefore, completely relaxed. Hence, the tests were conducted with two single harmonic (pure sinusoidal) control signals, namely at the $\Omega p = \omega = 1/\text{rev}$ and $2/\text{rev}$ frequencies. For these two control frequencies, the control phase angle with respect to the fan centerline was then varied from $\phi = -180$ to $\phi = +180$ degrees. The results of for this phase angle sweep for both the 1/rev and 2/rev cases are presented in Figs. 13 and 14, respectively. The best phase results at the three tested spinning rates for the attenuation of the 2/rev harmonic (which would not interfere with the rotor cyclic control) is collected in Fig. 15. The overall best result occurred at 750RPM and exceeds the respectful 80% attenuation value for the 2/rev frequency. It also little affects the fundamental frequency, 1/rev. In general, the best performance for decreasing the vibration at 2/rev was achieved with a leading control phase angle (negative azimuth) between -90 and -45 degrees, depending on the control frequency. As expected, this corresponds to a position just before reaching the transverse flow delivered by the fan.

In all cases, the calibrated vibration levels were measured by the Hall sensor located at the base of the APL for the first 8 harmonics of the blade fundamental frequency and they were repeatable. The signals were recorded in absolute dB levels for both the baseline case (reference) and the open-loop control case and then transformed into the peak-to-peak percentage attenuation ratios shown in the figures. In all figures, negative values indicate an increase in the vibration levels compared to the baseline case. Some of the increased levels at higher harmonics (above 3/rev) were very high but it should be noted that the baseline levels for these

harmonics were not significant, as indicated in Fig. 12. Most importantly, the present results confirm the vibration spectrum reshaping generated by the APL, extracting energy from one harmonic and shifting it at other harmonics. This feature should be explored to develop effective closed-loop control algorithms to decrease the vibration transmissibility from the rotating to the non-rotating frame in real helicopter rotors at their critical frequencies.

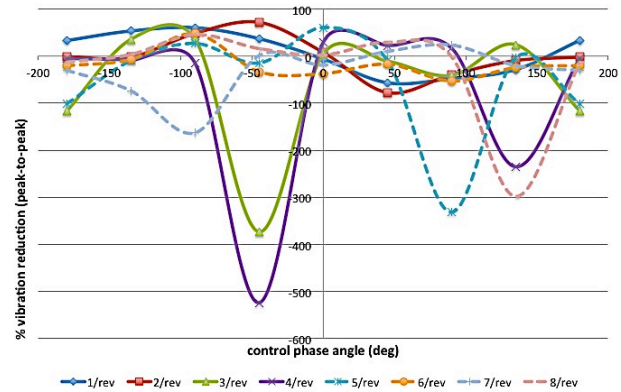


Fig. 13: 1/rev control signal – phase sweep effect.

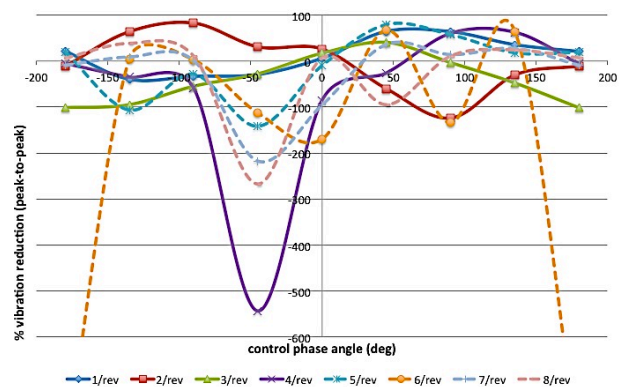


Fig. 14: 2/rev control signal – phase sweep effect.

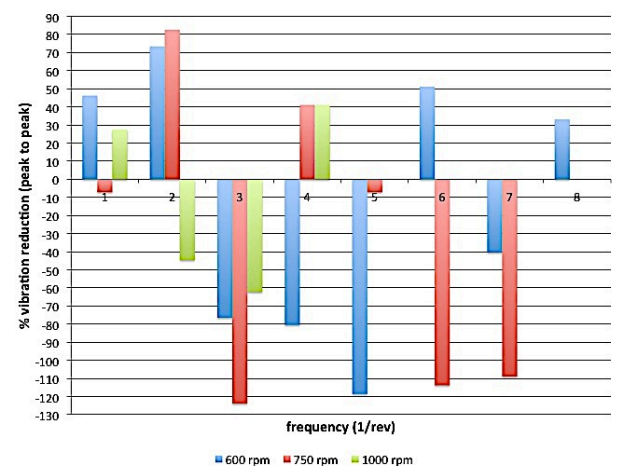


Fig. 15: APL best performance at different rotor spinning ratios (2/rev control frequency).

Although the APL is not a damping device, studies must be made in order to identify the impact of the friction on the performance. In the theoretical background presented in Section 2.1, the frictional force, $vN(t)$ shown in Fig. 1 was not modeled. This force is responsible for the Coulomb frictional effect that makes the effective stiffness of the “smart” spring a complex-valued quantity, $k = \text{Re}(k) + i\text{Im}(k)$. The imaginary part is expected to introduce secondary lags in the response spectrum, equivalent to introducing the velocity term in Hill’s equation, (3). Hence, in Fig. 16, the sliding effect at the actuator partially clamped situations (50% of locking force condition) is presented for the first 3 harmonics with the control frequency, set at 2/rev, indicating that the spectrum redistribution is in fact largely sensitive to this feature as well and, therefore, further development is necessary to be able to regulate closed-loop control schemes for this effect.

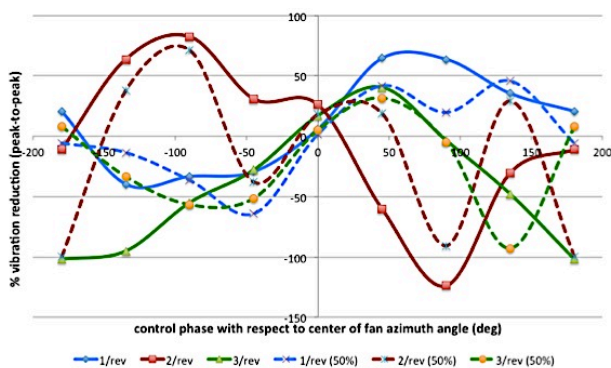


Fig. 16: 2/rev control signal – phase sweep effect for the completely clamped and partially clamped APL situations.

4. ACTIVELY CONTROLLED FLAP CONTROL ALGORITHM DEVELOPMENT

A novel control algorithm design framework that provides accurate reduced-order models to design time-periodic controllers for helicopter vibration suppression will be reported in this section. In this work, the reduced-order models were directly identified from high-fidelity coupled aeroelastic simulations rather than assembling initially uncoupled reduced-order models for the structural dynamics and aerodynamics. In this approach, a coupled aeroelastic model obtained from a comprehensive computational fluid dynamics (CFD) and computational structural dynamic (CSD) computer code defined the system, as described in Section 4.1. Since coupled CFD/CSD aeroelastic simulations can only provide input/output relationships of the helicopter aeroelastic system, mathematically tractable models were directly obtained from the detailed system identification. Very importantly, periodicity of the helicopter rotor aeroelastic response in the forward flight regime was

fully modeled and no assumptions or simplifications were made a priori. Furthermore, the proposed approach is directly transferrable to an experimental setting to cope with on-line identification and real-time controllers. It can be applied to IBC using active pitch links, flaps, twist actuation and higher-harmonic control of using the swashplate. Following the system identification, time-periodic models are generated in Section 4.2 to obtain an accurate map between control actuation and helicopter aeroelastic response in forward flight, and a fully periodic controller will be developed in Section 4.3.

4.1. High-fidelity aeroelastic code

The high-fidelity coupled aeroelastic analysis of helicopter rotor system equipped with trailing edge flaps was carried out using the in-house computer code, General Unsteady Vortex Particle (GENUVP) / General Aerodynamic and Structural Tool (GAST). Carleton University’s Rotorcraft Research Group has extensively used the GENUVP/GAST code for helicopter rotor system aeroelastic and aeroacoustic time-domain simulations.^[11,12] It was first developed at the National Technical University of Athens (NTUA) and validated in comparison with experimental data by NTUA for different flight regimes.^[13,14] The aerodynamic component of the code, GENUVP is a panel method code utilizing a vortex-particle free wake model for calculating the flow field around multi-component configurations. For the viscous effects, an a posteriori correction scheme is applied to the loads based on the ONERA model. The basis of GENUVP code is the Helmholtz decomposition principle, in which the flow field is decomposed into its irrotational and rotational components. The vortices released by the panels are straight-segmented vortex sheets when they are shed in the near field. Subsequently, the vorticities that these sheet segments carries are integrated to form vortex particles, which are convected into the far field, following a Lagrangian representation of the flow. The outputs of the GENUVP code are the aerodynamic loads and moments calculated with respect to the blade local coordinate system. When the aerodynamic loads are applied, the blade undergoes both rigid-body displacements and elastic deformations. These structural deformations are calculated using the structural component of the aeroelastic code, called GAST. In GAST, a beam model represents the flexible blade under large deformations with a second-order accuracy. For the solution, the equation of the beam model is discretized using the finite element method. The dynamic and structural coupling of the flexible components is performed in the context of a multi-body analysis. Hence, the beam undergoes out-of-plane (flapping) and in-plane (lead-lag) bending, extension and torsional deflections along with its rigid translations and rotations.

For the purpose of developing the time-periodic

reduced-order model and subsequent controller synthesis, the SHARCS blade configuration was used.^[15] This dynamically scaled, 1-m span, hinged rotor blade operates at the baseline forward-flight regime with the rotational speed of $\omega = 162.8$ rad/s and an advance ratio of $\mu = 0.28$ to produce the target tip Mach number of 0.52. The swashplate settings satisfied in the simulations the wind tunnel test trim condition. The trust coefficient to rotor solidity ratio was selected for typical forward flight regimes, $c_t/\sigma = 0.075$. The forward shaft tilt angle of was taken as 3 degrees. The collective, θ_0 , cyclic, θ_{1s} and θ_{1c} swashplate settings that satisfy the mentioned trim condition were obtained in the simulations, and produced the values of 5.42 degrees, -3.72 degrees and 1.44 degrees, respectively. These settings were kept constant in the entire development. In addition, the blades were assumed identical, and the elasticity of the shaft and the swash plate was not modeled.

For the aerodynamic calculations, the flow was assumed attached, and the vortices were emitted from both the trailing edge of the blade and the gap between the blade and the flap. No drag correction was performed and only rigid flap deflections were imposed. Hence, both the dynamics of the flap structure and its actuation mechanism were not included in this study.

4.2. Linear Time Periodic system identification

The system identification was carried out to obtain the effect of the trailing edge flap on the helicopter blade (rotating frame) loads, namely the vertical shear, F_z and blade pitch moment, M_y , around a pre-defined baseline condition defined by the advance ratio and trimmed swashplate settings. The model was assumed to be Linear and Time Periodic (LTP). Figure 17 shows the definition of the blade loads and hub loads used in this study.

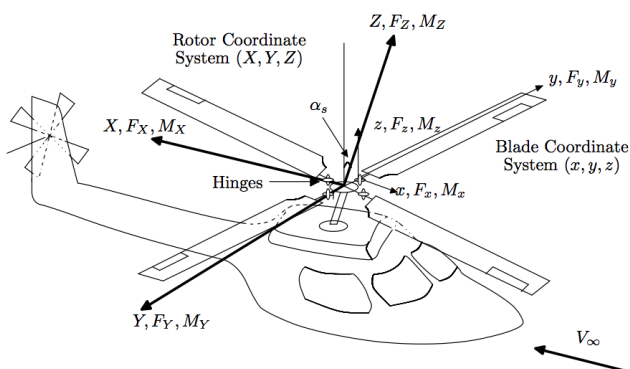


Fig. 17: Helicopter reference systems.

The LPT model of the system was obtained in state-space form from the input/output data of the system

utilizing the Subspace Identification Method (SIM).^[16] SIM does not require precise, a priori, knowledge of the model parameters. Therefore, a more efficient system identification using shorter experimental and/or computational input/output data sets is possible. In addition, the SIM method offers the flexibility of using ensemble data obtained from several independent aeroelastic simulations. Since high-fidelity computational tools demand higher computational time as the simulation time evolves (in GENUVP the number of particles accumulate), by simulating shorter periods the computational time was significantly reduced.

In the GENUVP/GAST aeroelastic simulations, one full rotation was divided into 24 equally spaced intervals as shown in Fig. 18. Physically realizable random deflections were given to the flap of the first blade with a maximum amplitude of 5 degrees at each discrete azimuth location, $\Psi_{\{k=1,2,\dots,24\}} = 0, 15, \dots, 345$ degrees, with $\Delta\Psi = 15$ degrees. The flap deflection along the interval $\Delta\Psi$ was kept constant to satisfy a zero-order-hold assumption used in the discretization process. Since GENUVP/GAST requires a finer azimuth resolution to solve for the helicopter aeroelastic response, each azimuth interval $\Delta\Psi$ was then divided into three to match the required sampling rate of the GENUVP/GAST simulations, $\delta\Psi = 5$ degrees (Fig. 18).

It was further observed that ignoring the interactions of the blades when the flaps of all blades were deflected leads to significant errors at some specific frequencies, such as 3/rev. Hence, an all-blade analysis that included the interaction of the blades through the disturbed wake shed the flaps was shown to be important for the correct modeling of the discrete linear LTP state-space system. The flap shed vortices introduce significant time-delays in the system that need to be included the control design. This all-blade model finally provided a fair map between the flap deflections of one blade, δ_{1k} (for example for blade $j = 1$) and the selected loads, measured in the rotating frame, at all four blades: $F_{z,jk}$ and $M_{y,jk}$ ($j = 1, \dots, 4$) and at every discretized azimuth angle location, k ($k = 1, \dots, 24$).

Since the described model includes the dynamics of all blades, the order of the LTP system had to be increased. The final augmented state-space representation contained the outputs of the rotating frame blade loads caused by the deflection of all flaps individually. The performance for this 48-states LTP reduced-order system is presented in Fig. 19 along with the results for the simplified one-blade model. The reference is the complete model simulation, GENUVP/GAST. To obtain the total hub loads in the non-rotating frame, F_X , M_X and M_Y (as defined in Fig. 17) standard coordinate transformation was applied to the rotating frame

blade loads according to the blade azimuth location.

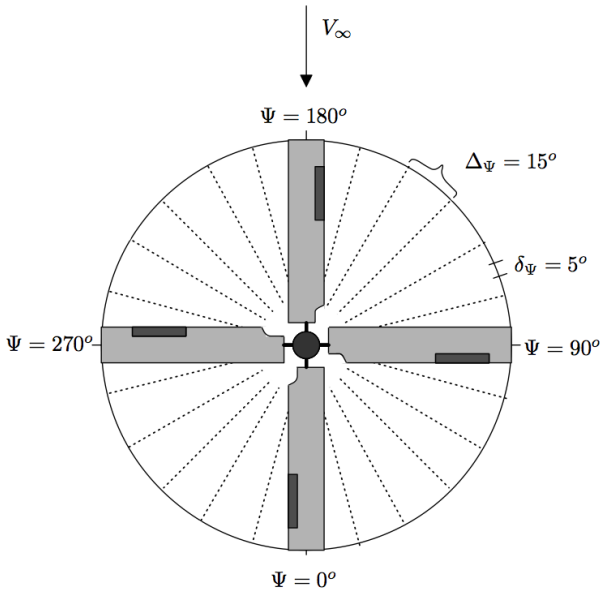


Fig. 18: Data sampling scheme used in the system identification process.

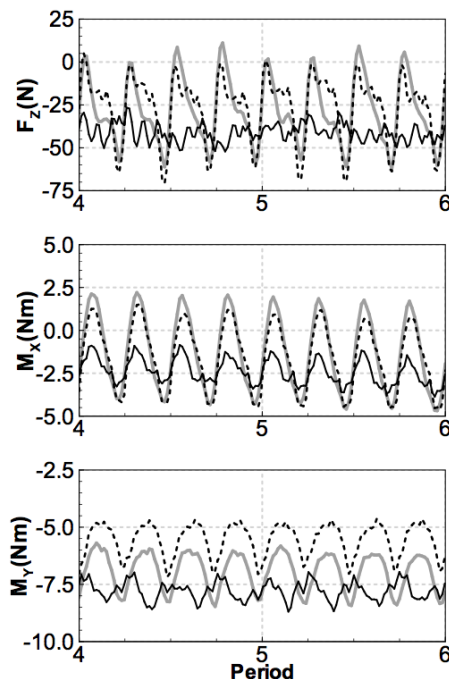


Fig. 19: Total hub loads predictions in the non-rotating frame due to all 4 flaps ($j = 1, \dots, 4$) 6-degrees deflections at 1/rev, with 90-degrees phase shifts, i.e. $\delta_j(t) = 6 \sin(\Omega t + (j-1)\pi/2)$. GENUVP/GAST reference model (gray), LPT one-blade model (black) and LPT all-blades model (dashed).

4.3. Linear Time Periodic controller

Helicopter vibration control studies have commonly used T -matrix algorithms for Higher Harmonic Control (HHC).^[17] The T -matrix is the sensitivity matrix between the control input from the rotor

swashplate or trailing edge flaps in the present case and the matrix outputs are the blade and hub loads. The control action includes the adaptive estimation or identification of the T -matrix. The estimation of the T -matrix can be carried out using Kalman filter and/or recursive least squares for either online or off-line applications. Since the steady T -matrix was shown to be equivalent to the time-invariant part of the Harmonic Transfer Function, HTF, classical frequency-domain system identification techniques have also been used with the T -matrix.^[18] The fundamental assumption of the T -matrix algorithm is that the helicopter dynamics can be modeled as Linear Time Invariant (LTI). It also assumes that the response of a helicopter to higher harmonic inputs is quasi-steady.^[19] Next, minimizing the quadratic cost function to regulate the helicopter vibratory hub loads usually carries out the controller design. Linear Quadratic Regulators (LQR) and Linear Gaussian Regulators (LQG) are the commonly used controller design techniques for helicopter vibration control.^[18-20] Both techniques depend heavily on the accurate estimation of the T -matrix.

In the implementation of the controller, after the control signal is applied, the signal is kept constant during the entire interval, which is generally taken as one revolution or one-quarter of the revolution for four-bladed rotors. Recently, another Periodic HHC (PHHC) controller using the T -matrix has been implemented.^[19] Still another research focused on the design of LQG controllers based on a LTP transfer function from the solution of the continuous-time periodic Riccati equations for the control of vibration caused by dynamic stall.^[20] T -matrix based optimal controllers have also been designed for helicopter vibration control using trailing edge flaps, where the quadratic cost was defined to minimize both the flaps deflection and the hub loads.^[21] In this latter work constant feedback controllers were obtained based on both the estimated T -matrix and cost function weights.

At a trimmed baseline case, for example for a four-bladed rotor system, only the harmonics of 4/rev vibratory vertical loads at the rotating frame of each blade, $F_{z,j}$ are in phase; the other harmonics cancel out due to the phase differences between them. Therefore, to suppress, for example, the 4/rev and 8/rev vertical hub loads, F_z , it is necessary to suppress the 4/rev and 8/rev components of the individual vibratory vertical blade loads, $F_{z,j}$ in the rotating frame. Alternatively, it is necessary to create precise phase differences at the 4/rev and 8/rev frequencies between the blades to cancel each other out in the non-rotating frame. On the other hand, to suppress the 4/rev and 8/rev hub roll and pitch moments, M_x and M_y , it is also necessary to suppress the 3/rev, 5/rev and 7/rev, 9/rev vibratory rotating frame bending moment, $M_{x,j}$ and pitching moment, $M_{y,j}$ because the transformation of the

rotating frame blade loads with frequency content of 3/rev, 5/rev and 7/rev, 9/rev induces 4/rev and 8/rev non-rotating frame hub roll and pitch moments. Therefore, for a 4/rev suppression, both the 3/rev and 5/rev frequency components of the rotating frame moments generated by the flap deflection need to be suppressed as well due to their higher-harmonic contributions to the hub roll and pitch moments, M_x and M_y . In addition, in order to maintain the same trim state for the rotor, the 1/rev components of the flap bending and pitching moments in the rotating frame need to be balanced.

In the present work, to suppress the rotating frame loads all design weights were taken the same for all blades, and the performance weight was selected to decrease vibrations at some specific frequency. This type of approach, however, did not guarantee that the hub loads in the non-rotating frame were suppressed. When the suppression of blade loads and/or hub loads was sought, a four-blade analysis as described in the previous section was required.

In the controller synthesis problem formulation, either the baseline disturbances can be given to each blade in the rotating frame or n/rev disturbances can be introduced in the non-rotating frame. The former necessitates the measurement of rotating frame blade loads or hub loads, while the latter requires the measurement of the hub loads only. To satisfy the rank constraints of the H_2 controller design method, regularization is also needed.^[22] If only the hub load disturbances are introduced in the non-rotating frame, the controller is prone to fail since it cannot detect the source of the vibration. If the baseline disturbances are given to each blade, then the phase shift between the disturbances should be included in the disturbance weight.

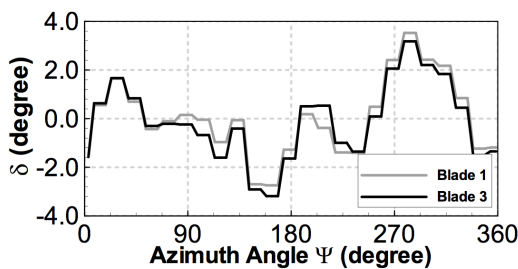


Fig. 20: Flap deflections (blades 1 and 3) for the 4/rev control of the vertical hub load, F_z .

The common approach to synthesize the time-periodic controller is two folded: first obtain the time-invariant representation of the system, and then use time-invariant controller design methods to design the controller. Although the resultant controllers are time-periodic, in their implementation it is necessary to wait for a full period to be completed to gather data, which results in unwanted time delays. A more

powerful method was followed in this study, to directly design the time-periodic controllers based on the state-space matrices available at every time step during one full period. The solution of the discrete-time periodic Riccati equation requires then special algorithms.^[23] Although many software packages provide a solution to time-invariant Riccati equation, no accessible algorithm for the solution of the time-periodic Riccati still exists.^[24] Therefore, an in-house discrete-time solver was developed.^[15]

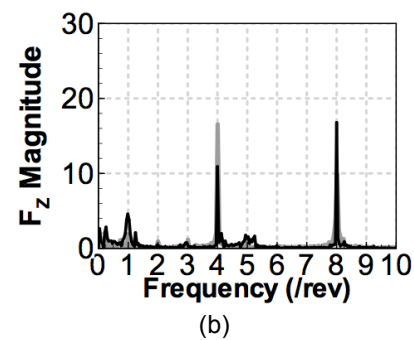
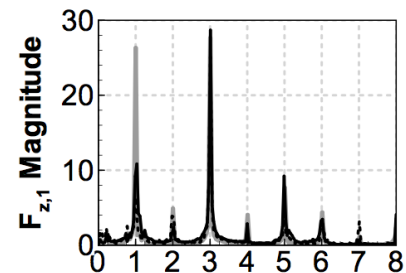
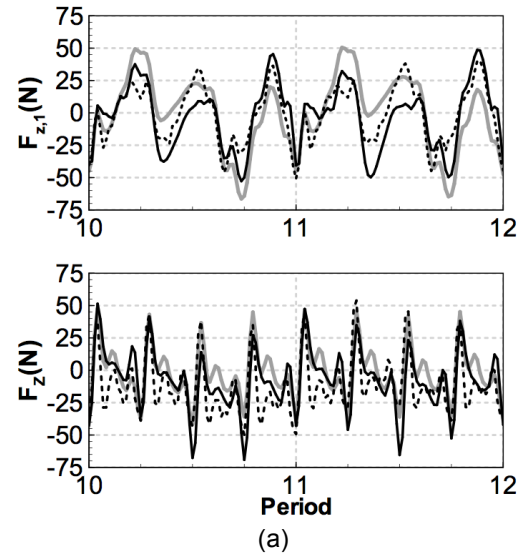


Fig. 21: Closed-loop control of the 4/rev vertical blade load, $F_{z,1}$ (rotating frame, blade 1) and total hub load, F_z . Baseline (gray) and controlled blade loads obtained with the reduced-order model (dashed) and the GENUVP/GAST simulations (black) in the (a) time-domain and (b) frequency domain.

The system reduced-order model obtained from the all blade LTP model of order 48 (see Section 4.2) in the four-blade configuration was used as the nominal plant. The performance weight for the measured output was selected to minimize the vibratory rotating frame blade load, F_z specifically at the 4/rev frequency. The disturbance weight included the baseline disturbances in the frequency range 0 to 5/rev and it was taken to be the same for all blades, i.e. with no phase difference. The obtained H_2 controller was applied in the closed-loop configuration and simulations were performed both using the GENUVP/GAST and the reduced-order model. The control flap deflections reached a steady-state value after four revolutions. Figure 20 shows the control TEF typical deflections, obtained from the closed-loop GENUVP/GAST simulations. The results of the closed-loop simulations are summarized in Fig. 21(a) – time domain, and Fig. 21(b) – frequency domain, from both the open-loop and closed-loop control simulations for the rotating frame vertical blade load, $F_{z,1}$ and the total hub load, F_z . The non-rotating frame blade load, F_z was suppressed at the 1, 2 and 4/rev frequencies by 59%, 52%, and 30%, respectively. While there was not any significant excitation recorded at 3/rev, the amplitudes at the frequencies of 5 and 8/rev were increased by 20% and 67%, respectively. On the other hand, the amplitudes at the frequencies of 6, 7 and 9/rev were reduced by 21%, 36% and 40%, respectively. From Fig. 21(a), it can also be seen that the reduced-order model predictions are in fair agreement with the high-fidelity code, GENUVP/GAST results.

5. CONCLUSIONS

In the present paper, recent developments of the blade stiffness and flow control devices envisioned in the SHARCS (Smart Hybrid Active Rotor Control System) project were reported. In particular, the stiffness control device (active pitch link) was tested both in the bench and at the whirl tower and vibration reductions in the rotating frame of near 90% at 2/rev were verified in the single-blade articulated rotor configuration. The active pitch link introduced angles of attack in the order of 0.1 degrees in the blade, indicating that helicopter rotor vibration can be achieved without introducing significant modifications in the blade angle of attack, in a novel and promising approach for individual blade control. Also in the paper, a framework for designing the control algorithms for the flow control device of SHARCS – the actively controlled flap was described using reduced-order models based on a high-fidelity aeroelastic code. For the first time, a fully periodic controller valid for significant forward-flight advanced ratio was developed. Most of the closed-loop control simulations obtained from the

reduced-order model and the full-order high-fidelity aeroelastic simulations provided similar results with few exceptions, also indicating the accuracy of the reduced-order model. It was verified in the simulations that the vibration suppression of both the rotating frame and hub loads were attained without causing detrimental changes in the rotor trim state values or exceeding the allowable flap deflections, typical to current designs.

6. ACKNOWLEDGEMENTS

The authors would like to acknowledge the contributions from other research partners in SHARCS, in special to Dr. Michael Rose from the German Aerospace Center, DLR's Institute of Composite Structures and Adaptive Systems for key contributions in the development of the in-house Riccati equation solver. The authors would also like to acknowledge the valuable contributions of Prof. Giuliano Coppotelli and Ms. Chiara Grappasonni from University of Rome "La Sapienza" in the active pitch link data acquisition during the whirl tower tests. Acknowledge is also due to NTUA, the Technical University of Athens, especially to Prof. Spyros Voutsinas and Dr. Vassilis Riziotis for their fundamental contributions in the modeling of the flap in the GENUVP/GAST code.

7. REFERENCES:

1. Nitzsche, F., "A New Individual Blade Control Approach to Attenuate Rotor Vibration," Paper No. 8, Vol. I., *Proceedings: 22nd European Rotorcraft Forum*, Brighton, UK, 1996.
2. Nitzsche, F., "Smart Spring Actuation for Helicopter Individual Blade Control: A Frequency Domain Analysis," *Seventh International Conference on Adaptive Structures and Technologies*, Rome, Italy, 1996, P. Santini, C. A. Rogers, Y. Morotsu, Editors, Technomic, Lancaster, PA, 1997, pp. 331-341.
3. Nitzsche, F., "Modeling an Adaptive Impedance Boundary Condition Device for Helicopter Individual Blade Control," *SPIE 4th Annual Symposium on Smart Structures and Materials*, San Diego, CA, 1997, V. V. Varadan, Editor, The International Society for Optical Engineering, Vol. 3039, pp. 216-226.
4. Nitzsche, F., Zimcik, D., Wickramasinghe, V. and Yong, C., "Control Laws for an Active Tunable Vibration Absorber Designed for Aeroelastic Damping Augmentation," *The Aeronautical Journal of the UK Royal Aeronautical Society*, Vol. 108, No. 1079, 2004, pp. 35-42.

5. Young, C., Zimcik, D.G., Wickramasinghe, V.K. and Nitzsche, F., "Development of the Smart Spring for Active Vibration Control of Helicopter Blades," *Journal of Intelligent Material Systems and Structures*, Vol. 15, 2004, pp. 37-47.
6. Oxley, G., Nitzsche, F. and Feszty, D., "Smart Spring Control of Vibration on Helicopter Rotor Blades," *AIAA Journal of Aircraft*, Vol. 46, No. 2, 2009, pp. 692-696.
7. Nitzsche, F., Harold, T., Wickramasinghe, V.K., Young, C. and Zimcik, D.G., "Development of a Maximum Energy Extraction Control for the Smart Spring," *Journal of Intelligent Material Systems and Structures*, Vol. 16, No. 11/12, 2005, pp. 1057-1066.
8. Nitzsche, F. et al, "The SHARCS Project: Smart Hybrid Active Rotor Control System for Noise and Vibration Attenuation of Helicopter Blades," Paper No. 52, *Proceedings: 31st European Rotorcraft Forum*, Florence, Italy, 2005.
9. Kloeppel, V. and Enenkl, B., "Rotor Blade Control by Active Helicopter Servo Flaps" Paper No. IF-158, *Proceedings: International Forum on Aeroelasticity and Structural Dynamics*, Munich, Germany, 2005.
10. Splettstoesser, W.R. et al, "The HELINOISE Aeroacoustic Rotor Test in the DNW – Test Documentation and Representative Results," DLR-Rept. No. 93-09, German Aerospace Center, (DLR), Braunschweig, Germany, 1993.
11. Nitzsche, F. and Opoku, D.G., "Acoustic Validation of a New Code Using Particle Wake Aerodynamics and Geometrically Exact Beam Structural Dynamics," *The Aeronautical Journal of the UK Royal Aeronautical Society*, Vol. 109, No. 1096, 2005, pp. 257-267.
12. Cesnik, C.E.S., Nitzsche, F., Opoku, D.G. and Cheng, T., "Active Twist Rotor Blade Modelling Using Particle-Wake Aerodynamics and Geometrically Exact Beam Structural Dynamics," *Journal of Fluids and Structures*, Vol. 19, 2004, pp. 651-668.
13. Voutsinas, S. and Triantos, D.G., "High Resolution Aerodynamic Analysis of Full Helicopter Configurations," Paper No. C-11, *Proceedings: 25th European Rotorcraft Forum*, Rome, Italy, 1999.
14. Voutsinas, S. et al, "Aerodynamic Interference in Full Helicopter Configurations and Assessment of Noise Emission: Pre-test Modelling Activities for the HELINOVI Experimental Campaign," *Proceedings: 31st European Rotorcraft Forum*, Florence, Italy, 2005.
15. Ulker, F.D., *A New Framework for Helicopter Vibration Suppression; Time-periodic System Identification and Controller Design*, Ph.D. thesis, Carleton University, 2011.
16. Verhaegen, M. and Yu, X., "A class of Subspace Model Identification Algorithms to Identify Periodically and Arbitrarily Time-varying Systems," *Automatica*, Vol. 31, No. 2, 1995, pp. 201-216.
17. Patt, D., Liu, L., Chandrasekar, J., Bernstein, D., and Friedmann, P., "The HHC Algorithm for Helicopter Vibration Reduction Revisited," 45th AIAA/ASME/ASCE/AHS/ASC Structures, Structural Dynamics and Materials Conference, 2004.
18. Wereley, N., *Analysis and Control of Linear Periodically Time Varying Systems*, Ph.D. thesis, Massachusetts Institute of Technology, February 1991.
19. Malpica, C., *Contributions to the Dynamics of Helicopters with Active Rotor Controls*, Ph.D. thesis, University of Maryland, College Park, 2008.
20. Depailler, G., *Alleviation of Dynamic Stall Induced Vibrations in Helicopter Rotors using Actively Controlled Flaps*, Ph.D. thesis, The University of Michigan, 2002.
21. Liu, L., Friedmann, P., Kim, I., and Bernstein, D., "Rotor Performance Enhancement and Vibration Reduction in Presence of Dynamic Stall using Actively Controlled Flaps," *American Helicopter Society Journal*, Vol. 53, No. 4, 2008, pp. 338-350.
22. Chen, T. and Francis, B., *Optimal Sampled-Data Control Systems, Communication and Control Engineering Series*, Springer-Verlag, 1995.
23. Bittanti, S., Laub, A. and Williams, J., *The Riccati Equation*, Springer-Verlag, 1991.
24. Varga, A., "A Periodic Systems Toolbox for Matlab," *Proceedings: IFAC'05 World Congress*, Prague, Czech Republic, 2005.